Optics Communications 441 (2019) 45–48

Contents lists available at ScienceDirect

Optics Communications

journal homepage: www.elsevier.com/locate/optcom

High-visibility underwater ghost imaging in low illumination

Ying Zhang, Wendong Li, Hengze Wu, Yihai Chen, Xiaoyi Su, Ya Xiao, Zhaoming Wang, Yongjian Gu *

Department of Physics, Ocean University of China, Qingdao 266100, China

ARTICLE INFO

Keywords:
Underwater ghost imaging
Attenuation
Longer-distance underwater imaging

ABSTRACT

Underwater imaging is a challenging topic in the field of photography due to the absorption and scattering of light by water, which reduces the imaging distance and visibility. In this paper, the effects of seawater on the quality of ghost imaging (GI) are analyzed theoretically and experimentally. Our results indicate that GI technique, to a certain extent, can achieve better imaging quality than conventional imaging, especially under weak light condition in seawater environments. The compressed sensing ghost imaging (CSGI) can further enhance the visibility of ghost images with fewer measurements. Therefore, ghost imaging has the potential of realizing longer-distance underwater imaging, owing to its robustness against seawater environmental disturbance.

1. Introduction

Underwater imaging [1,2] is a crucial technology for many ocean-related applications, such as underwater navigation, surveying, and mining. Due to the strong absorption and scattering of light in underwater media, underwater imaging has encountered many difficulties. Ghost imaging (GI) [3–6], as a new imaging method, recovers the information of the object utilizing the correlation of intensity fluctuations between two output beams. The object beam interacts with the object without providing any spatial information, whereas the reference beam provides spatial information without interacting with the object. Compared with traditional imaging, GI shows great potential in optically harsh or noisy environments, and has the advantages of achieving high resolution beyond the Rayleigh diffraction limit [7], and GI is also free from outside disturbance and robust to turbulence [8,9].

GI has attracted increasing much attention in the fields of optical imaging and remote sensing in the past decades. In 1988, D. N. Klyshko [10] first proposed a theoretical correlation imaging scheme using entangled photon pairs, which was later realized by T. B. Pittman [3]. Later, it was found that a form of ghost imaging is possible with pseudo-thermal light [4]. In order to achieve better reconstruction results, it usually requires a larger number of measurements and takes much more computation time. Many protocols and algorithms have been proposed to improve the quality and speed of ghost imaging, such as higher-order correlations [11], compressed sensing GI (CSGI) [12], differential GI (DGI) [13]. Compared with conventional GI algorithm, the DGI algorithm can remove the background and enhance the signal-to-noise ratio (SNR), especially for imaging weakly absorbing objects or objects in scattering media [13,14]. CSGI was shown to be able to reconstruct high quality ghost images benefiting from the sparsity of the object [15]. They were extended to many applications including biomedical imaging [16], remote ghost imaging lidar [17], and cryptography [18].

Although the research of GI in air has achieved great success, the underwater ghost imaging is rarely explored. In underwater conditions, photons will suffer from energy dissipation due to attenuation caused by suspended particulates as well as fading caused by turbulence in underwater environments, restricting traditional underwater imaging to short ranges. The influences of atmospheric turbulence and scattering media on GI were discussed in previous studies [9,19–22]. In seawater environments, because of absorption and scattering, the light field becomes weaker with the increase of transmission distance. The effects of underwater turbidity on computational GI were investigated recently [23], and the results show that GI has the advantage of a turbidity-free and wider angle of view. However, in all the studies mentioned above, the properties of GI operating in low illumination through seawater have not previously been investigated. At present, it is not clear whether underwater GI can still yield high-contrast images under weak light. In this paper, we focus on the light attenuation in seawater, and exploring the GI of a double-slit under weak light. Besides the theoretical analysis of the effect of attenuation, we compare experimentally the images generated by several kinds of GI algorithms with traditional imaging techniques. Our results show that the GI system is more robust to weak receiving light though seawater media than conventional optical imaging under similar conditions.

* Corresponding author.
E-mail addresses: liwd@ouc.edu.cn (W. Li), yjgu@ouc.edu.cn (Y. Gu).

https://doi.org/10.1016/j.optcom.2019.02.036
Received 19 December 2018; Received in revised form 13 February 2019; Accepted 14 February 2019
Available online 19 February 2019

2. The effects of attenuation on GI

The ghost image $G(x)$ can be retrieved by calculating the second-order correlation function of the intensity fluctuations between the intensity distribution $I_r(x)$ on the reference detection plane and the total intensity S recorded on the bucket detector plane

$$G(x) = \langle S I_r(x) \rangle - \langle S \rangle \langle I_r(x) \rangle, \tag{1}$$

where $\langle \cdots \rangle$ is an average over multiple measurements. When no attenuation in the channel, supposing that $I_t(x')$ is the intensity distribution of illumination on the object, and $T(x')$ indicating the transmission function of the object, the total intensity of light received by the bucket detector can be calculated as

$$S = \int I_t(x') T(x') dx'. \tag{2}$$

When the light passes through the seawater channel, the light field is greatly disturbed due to the water absorption and scattering. Now the light intensity distribution on the object $I_{tsca}(x')$ would has two components, the direct transmission light intensity $\alpha I_t(x')$ and the scattered light intensity $I_{sca}(x')$. Therefore $I_{tsca}(x')$ can be expressed as

$$I_{tsca}(x') = \alpha I_t(x') + I_{sca}(x'), \tag{3}$$

Where α represents the transmission ratio of seawater, which is approximately a constant. Noticing besides scattering, the seawater media may causes attenuation to the light intensity. Thus we modify the theory developed in Chen's paper [24], the total intensity of light on the bucket detector can be written as

$$S_{sca} = \eta \int I_{tsca}(x') T(x') dx' = \eta \int [\alpha I_t(x') + I_{sca}(x')] T(x') dx', \tag{4}$$

where η is also approximately a constant, indicating the transmission efficiency of the seawater channel between the object and the bucket detector. Inserting Eq. (4) into Eq. (1), the intensity correlation can be expressed as follows

$$\begin{aligned} G_{sca}(x) = \eta \int [\langle I_r(x) I_{sca}(x') \rangle - \langle I_r(x) \rangle \langle I_{sca}(x') \rangle] T(x') dx' \\ + \eta\alpha \left[\langle I_r(x) S \rangle - \langle I_r(x) \rangle \langle S \rangle \right]. \end{aligned} \tag{5}$$

Since the phase of the scattered field is random, the scattering light and the reference optical field satisfying the relation $\langle I_r(x) I_{sca}(x') \rangle = \langle I_r(x) \rangle \langle I_{sca}(x') \rangle$. Then Eq. (5) reduces to

$$G_{sca}(x) = \eta\alpha G(x). \tag{6}$$

According to Eq. (6), although the brightness of GI images is decreased by a factor of $\eta\alpha$ due to the attenuation, the contrast and other characteristics of GI will be maintained, and high-quality images can be obtained because the distortion of the light field between light source and the object has no effects on ghost imaging.

3. Experimental description

We performed an underwater GI experiment to investigate the effects of attenuation. The schematic of the experimental system is shown in Fig. 1. To simulate underwater environments, we choose seawater in latitude and longitude 36°06′4″N, 120°54′12″E, with refractive index $n = 1.32$ as the liquid media. Since the blue–green optical window corresponds to the minimum underwater attenuation region, a light source of wavelength of $\lambda = 450$ nm is chosen in our experiment.

The pseudo-thermal source, which is realized by modulating a continuous laser beam with a rotating ground glass (RGG), is divided into a reference path and an object path by a 50/50 non-polarizing beam splitter (BS). The two beams pass through a container of length 45 cm filled with seawater. After the two paths are combined at the second BS_2, their signals are recorded by the same detector, which consists of a collection lens L_3 and a charged coupled device (CCD, Vieworks VC-2MC-M340E0, with resolution of 5.5 *um*). The bucket detector in the object path is replaced by the right-half of the CCD. A double-slit with width $a = 0.05$ mm and center-to-center separation $d = 0.45$ mm is placed in the object path. In order to locate the position of the double-slit, we temporarily placed the double-slit behind the BS_1, with the distance between BS_1 and object $z_r = 41$ mm. And then we adjusted the positions of L_3 and CCD to make a clear double-slit image on the CCD. This means that the positions of double-slit, L_3 and CCD detection plane should meet the Gaussian thin-lens equation. After that, we moved the object to the object path, with experimental parameters satisfying $z_r = z_1 + z_2$.

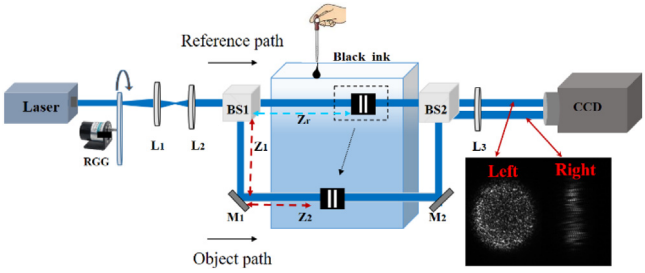

Fig. 1. Schematic of ghost imaging with pseudo-thermal light. The illustration shows the light intensity distribution taken by the CCD. The left half of the image shows the intensity distribution on the reference detection plane, whereas the right half of the image shows the intensity distribution on the object detection plane. Black ink is added into seawater to change the turbidity of the medium. RGG denotes rotating ground glass, L_1 ($f = 25$ mm), L_2 ($f = 50$ mm) and L_3 ($f = 200$ mm) are lenses, BS_1 and BS_2 denote non-polarizing beam splitters, M_1 and M_2 are reflective mirrors. CCD serves as detector in the reference and object path. . (For interpretation of the references to color in this figure legend, the reader is referred to the web version of this article.)

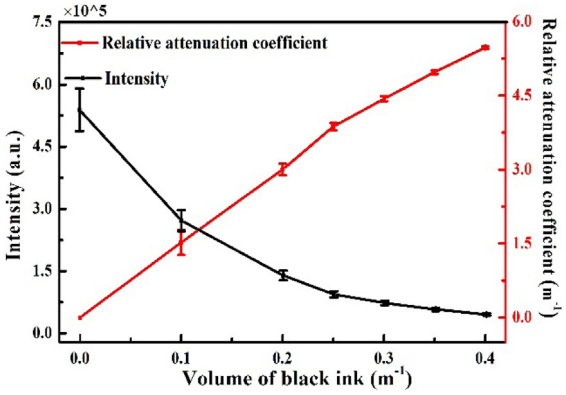

Fig. 2. Total intensity on the object detection plane averaged over 3000 measurements and the relative attenuation coefficient with increasing turbidity. The horizontal axis corresponds to the volume of black ink.

To investigate the effects of attenuation on GI, we introduce the turbidity by adding black ink into the seawater. The turbidity of seawater can be controlled by varying the volume of the black ink. Since the volume of ink is negligible compared to that of the seawater, the change of refractive index of the seawater due to the ink can be ignored. According to the Beer–Lambert law [25], the received light intensity I_1 through the seawater channel without ink can be described by $I_1 = I_0 e^{-cl_1}$, where I_0 is the intensity of transmitted light before entering the container, c is the attenuation coefficient of seawater, and $l_1 = 45$ cm is the underwater transmission distance. With the increase of turbidity, new attenuation effects will be introduced, and the relative attenuation coefficient Δc caused by the ink can be calculated by $I = I_1 e^{-\Delta c l_1}$. When the added black ink was 0 mL, 0.1 mL, 0.2 mL, 0.25 mL, 0.3 mL, 0.35 mL, and 0.4 mL, the received light intensity I can be measured, and the corresponding relative attenuation coefficients are shown in Fig. 2. The total intensities on the object detection plane in different turbidity are also reported in Fig. 2.

The error bars represent standard deviations after averaging over 3000 independent measurements. It is evident that the larger the relative attenuation coefficient, the stronger the absorption and scattering of light will be. It is mainly caused by the interaction of laser with molecules and particles in turbid seawater. The larger relative attenuation coefficient means more optical power consumption, which is consistent with the attenuation of laser through longer-distance underwater transmission with the same turbidity.

4. Experimental results and discussion

In experimenting we are not concerned with the output power of the light source, just concerned that whether the irradiance arriving to the CCD is visible. The double-slit images taken directly by CCD under the same experimental conditions are shown in Fig. 3(a). For the traditional underwater imaging, with the turbidity getting stronger, the signal has decreased. It is well-known that traditional imaging methods are based on the first-order correlation of light fields, and the spatial information of the object can be obtained only when the object is observed. Therefore, when an object is in a complex environment or the light is very weak, we cannot, in principle, accurately collect enough information about the object. In other words, the weak illumination may be invisible to CCD.

For pseudo-thermal GI, it is natural to argue that whether high resolution images could be obtained in the strong scattering or weak light conditions. The intensity distributions on the object detection plane are shown in Fig. 3(b). Since the pseudo-thermal light is incoherent, the diffraction pattern of the double-slit is not presented on the CCD camera. The speckle patterns on the reference detection plane, as plotted in Fig. 3(c), show the same variation trend with that of in Fig. 3(b), where the images are getting darker and darker until finally disappears with increase of turbidity. Fig. 3(d) and (e) show the images reconstructed using the conventional GI algorithm and the DGI algorithm after averaging over 3000 measurements. We can obtain DGI images with quality higher than those images obtained using conventional GI, and the DGI images have no obvious difference when the turbid seawater makes the light intensity weaker and weaker.

In order to clearly compare the performance of DGI and traditional imaging, we investigate the peak signal-to noise ratio (PSNR) [26] and the visibility [27], which are defined as

$$\mathrm{PSNR} = 10\log_{10}[\frac{(2^{m}-1)^{2}}{\mathrm{MSE}}], \tag{7}$$

$$\mathrm{Visibility} = \frac{\langle G_s\rangle - \langle G_b\rangle}{\langle G_s\rangle + \langle G_b\rangle}, \tag{8}$$

where G_s and G_b are the intensities of the image in the signal region and the background region, respectively. MSE represents the mean square error of the original image relative to reconstruction image. The PSNR and visibility are shown in Fig. 3(f) and (g). From the first point in the figures, it is obvious that the quality of ghost imaging is not better traditional imaging in pure seawater environments. This is because for a pseudo-thermal GI, the background noise resulting from the coincidences [28,29] may submerge the effective information of the image. When the turbidity of seawater is high, the traditional imaging technique is completely failed, so the last two points of in Fig. 3(f) and (g) could not be accurately calculated. The comparisons indicate that ghost imaging could maintain imaging quality in complex seawater environments, which is propitious to low-energy optical fields. But this advantage does not always exist, we also note that as the turbidity increases, the DGI images appear somewhat blurred, as shown in Fig. 3(e). This is because the spatially point-to-point coincidence between the object path and the reference path is decreased by a factor of $\eta\alpha$ in Eq. (6). To get better imaging results for the strong turbidity, more measurements should be performed, which require longer measurement time. Katz et al. [11] proposed that CSGI can improve the quality of recovered image with fewer measurements. The

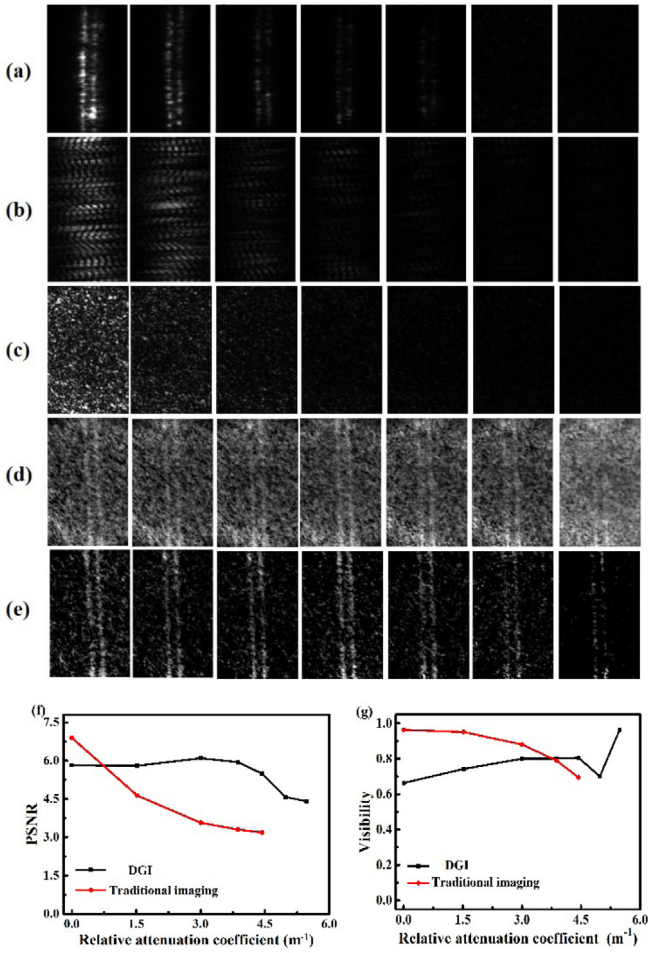

Fig. 3. Experimental results of imaging a transmission double slit with increasing turbidity. In panel (a)–(e), volumes of black ink from left to right are 0 mL, 0.1 mL, 0.2 mL, 0.25 mL, 0.3 mL, 0.35 mL, and 0.4 mL. (a) Traditional imaging of the double slit. (b) Images on the object detection plane captured by the right-half of the CCD. (c) The speckle fields on the reference detection plane recorded by the left-half of the CCD. (d)–(e) The images recovered via conventional GI and DGI after averaging over 3000 measurements. (f)–(g) The PSNR and visibility of the DGI (black lines) and traditional imaging (red lines). When the amount of ink added reaches to 0.35 mL and 0.4 mL, traditional imaging has completely failed, so the corresponding PSNR and visibility are not calculated. . (For interpretation of the references to color in this figure legend, the reader is referred to the web version of this article.)

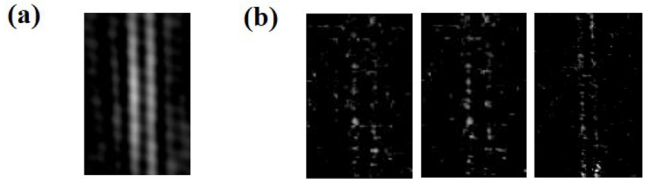

Fig. 4. (a) SCGI reconstruction with 1000 measurements and (b) DGI reconstructions in different measurements (M =1000, 2000, 3000, respectively), when adding 0.4 mL black ink into the seawater.

results for both DGI and CSGI reconstructions are plotted in Fig. 4. We found that the visibility of CSGI images can be significantly enhanced using the same number of measurements.

Let us elaborate a bit more on the advantages of GI in the weak light through the seawater channel. When the attenuation is strong, the traditional imaging will be affected by the transmission ratio of the media and the scattered light. But for ghost imaging, from Eq. (6), the seawater mainly affects the brightness of GI. The scattered light

illuminating the object will not affect the image quality. On the object detection plane, the total intensity is required, so the distortion of the light field between the object and the object detector has also no effects on ghost imaging performance. Furthermore, the bucket detector of ghost imaging system often employs the total intensity of spatial-resolution detector or a single pixel detector, which is technically easier to be used to improve the sensitivity than traditional imaging relying on the multi-pixel array information. Therefore, ghost imaging using second-order correlation is more sensitive to weak light and more robust to scattering. The advantage of weak light imaging is the same as that of entangled-photon ghost imaging [3], and a visible image can still be successfully obtained even at the single-photon level. Thus, the ghost imaging technique has potential applications in the underwater imaging over long distance and in muddy underwater environments, which may offer a better alternative for underwater optical imaging.

5. Conclusion

In our work, we firstly analyzed the effects of attenuation on underwater ghost imaging by the second-order correlation function. We then conducted a pseudo-thermal ghost imaging experiment across seawater channels with different turbidity. We further compared the visibility and PSNR of DGI to that of traditional imaging, and the experimental results show that the imaging quality with DGI is relatively good even at low level of illumination levels for CCD. We also found that the quality of underwater ghost imaging can be significantly improved by applying the method of compressed sensing. Since a larger attenuation coefficient is analogous to a longer transmission distance of light through water, the ghost imaging may be an effective method for long-range underwater imaging. In addition, ghost imaging is not sensitive to scattering, and therefore having the advantage for explorations in variable and harsh oceanic environments, such as around hydrothermal vent sites.

Acknowledgments

This work was funded by the National Natural Science Foundation of China (Grants No. 61701464, 61575180, and 11475160). The authors would like to thank Long-wen Zhou for the helpful suggestions and the language assistance.

References

[1] D.M. Kocak, F.R. Dalgleish, F.M. Caimi, Y.Y. Schechner, A focus on recent developments and trends in underwater imaging, Mar. Technol. Soc. J. 42 (1) (2008) 52–67.
[2] J.S. Jaffe, K.D. Moore, J. Mclean, A. AssociatesTucson, M.R. Strand, Underwater optical imaging: status and prospects, Oceanography. 14 (3) (2001) 66–76.
[3] T.B. Pittman, Y.H. Shih, D.V. Strekalov, A.V. Sergienko, Optical imaging by means of two-photon quantum entanglement, Phys. Rev. A 52 (5) (1995) 3429.
[4] F. Ferri, D. Magatti, A. Gatti, M. Bache, E. Brambilla, L.A. Lugiato, High-resolution ghost image and ghost diffraction experiments with thermal light, Phys. Rev. Lett. 94 (18) (2005) 183602.
[5] M. D'Angelo, A. Valencia, M.H. Rubin, Y. Shih, Resolution of quantum and classical ghost imaging, Phys. Rev. A 72 (1) (2005) 013810.
[6] R. Borghi, F. Gori, M. Santarsiero, Phase and amplitude retrieval in ghost diffraction from field-correlation measurements, Phys. Rev. Lett. 96 (18) (2006) 183901.
[7] P.A. Moreau, E. Toninelli, P.A. Morris, R.S. Aspden, T. Gregory, G. Spalding, R.W. Boyd, M.J. Padgett, Resolution limits of quantum ghost imaging, Opt. Express 26 (6) (2018) 7528–7536.
[8] C.L. Luo, J. Cheng, A.X. Chen, Z.M. Liu, Computational ghost imaging with higher-order cosh-Gaussian modulated incoherent sources in atmospheric turbulence, Opt. Commun. 352 (2015) 155–160.
[9] R.E. Meyers, K.S. Deacon, Y. Shih, Turbulence-free ghost imaging, Appl. Phys. Lett. 98 (11) (2011) 111115.
[10] D.N. Klyshko, Two-photon light: influence of filtration and a new possible epr experiment, Phys. Lett. A 128 (3–4) (1988) 133–137.
[11] K.W. Chan, M.N. O'Sullivan, R.W. Boyd, High-order thermal ghost imaging, Opt. Lett. 34 (21) (2009) 3343–3345.
[12] O. Katz, Y. Bromberg, Y. Silberberg, Compressive ghost imaging, Appl. Phys. Lett. 95 (13) (2009) 131110.
[13] F. Ferri, D. Magatti, L.A. Lugiato, A. Gatti, Differential ghost imaging, Phys. Rev. Lett. 104 (25) (2010) 253603.
[14] M. Bina, D. Magatti, M. Molteni, A. Gatti, L.A. Lugiato, F. Ferri, Backscattering differential ghost imaging in turbid media, Phys. Rev. Lett. 110 (8) (2013) 083901.
[15] L. Jiying, Z. Jubo, L. Chuan, H. Shisheng, High-quality quantum-imaging algorithm and experiment based on compressive sensing, Opt. Lett. 35 (8) (2010) 1206–1208.
[16] A.X. Zhang, Y.H. He, L.A. Wu, L.M. Chen, B.B. Wang, Tabletop x-ray ghost imaging with ultra-low radiation, Optica 5 (4) (2018) 374–377.
[17] N.D. Hardy, J.H. Shapiro, Computational ghost imaging versus imaging laser radar for three-dimensional imaging, Phys. Rev. A 87 (2) (2013) 023820.
[18] S. Yuan, J. Yao, X. Liu, X. Zhou, Z. Li, Cryptanalysis and security enhancement of optical cryptography based on computational ghost imaging, Opt. Commun. 365 (2016) 180–185.
[19] H.K. Ben, G. Brun, I. Verrier, L. Froehly, C. Veillas, High-resolution optical correlation imaging in a scattering medium, Opt. Lett. 26 (24) (2001) 1969–1971.
[20] W. Gong, S. Han, Correlated imaging in scattering media, Opt. Lett. 36 (3) (2011) 394–396.
[21] J. Cheng, Ghost imaging through turbulent atmosphere, Opt. Express 17 (10) (2009) 7916–7921.
[22] D. Shi, C. Fan, P. Zhang, J. Zhang, H. Shen, C. Qiao, Y. Wang, Adaptive optical ghost imaging through atmospheric turbulence, Opt. Express 20 (27) (2012) 27992–27998.
[23] M. Le, G. Wang, H. Zheng, J. Liu, Y. Zhou, Z. Xu, Underwater computational ghost imaging, Opt. Express 25 (19) (2017) 22859–22868.
[24] Y.K. Xu, W.T. Liu, E.F. Zhang, Q. Li, H.Y. Dai, P.X. Chen, Is ghost imaging intrinsically more powerful against scattering? Opt. Express 23 (26) (2015) 32993–33000.
[25] H.J. Okoomian, Underwater transmission characteristics for laser radiation, Appl. Opt. 5 (9) (1966) 1441–1446.
[26] C. Zhang, S. Guo, J. Cao, J. Guan, F. Gao, Object reconstitution using pseudo-inverse for ghost imaging, Opt. Express 22 (24) (2014) 30063–30073.
[27] C. Gao, X. Wang, Z. Wang, Z. Li, G. Du, F. Chang, Z. Yao, Optimization of computational ghost imaging, Phys. Rev. A 96 (2) (2017) 023838.
[28] V. Alejandra, S. Giuliano, D. Milena, Y. Shih, Two-photon imaging with thermal light, Phys. Rev. Lett. 94 (6) (2005) 063601.
[29] W. Gong, S. Han, Correlated imaging in scattering media, Opt. Lett. 36 (3) (2011) 394–396.